

**Morphodynamic adaptation of a tidal basin to centennial sea-level rise
The importance of lateral expansion**

Guo, Leicheng; Xu, Fan; van der Wegen, Mick; Townend, Ian; Wang, Zheng Bing; He, Qing

DOI

[10.1016/j.csr.2021.104494](https://doi.org/10.1016/j.csr.2021.104494)

Publication date

2021

Document Version

Accepted author manuscript

Published in

Continental Shelf Research

Citation (APA)

Guo, L., Xu, F., van der Wegen, M., Townend, I., Wang, Z. B., & He, Q. (2021). Morphodynamic adaptation of a tidal basin to centennial sea-level rise: The importance of lateral expansion. *Continental Shelf Research*, 226, Article 104494. <https://doi.org/10.1016/j.csr.2021.104494>

Important note

To cite this publication, please use the final published version (if applicable).
Please check the document version above.

Copyright

Other than for strictly personal use, it is not permitted to download, forward or distribute the text or part of it, without the consent of the author(s) and/or copyright holder(s), unless the work is under an open content license such as Creative Commons.

Takedown policy

Please contact us and provide details if you believe this document breaches copyrights.
We will remove access to the work immediately and investigate your claim.

1 **Morphodynamic adaptation of a tidal basin to centennial sea-level rise:**
2 **the importance of lateral expansion**

3

4 Leicheng Guo ^{a, *}, Fan Xu ^a, Mick van der Wegen ^{b, c},
5 Ian Townend ^d, Zheng Bing Wang ^{a, c, e}, Qing He ^a

6

7 ^a State Key Lab of Estuarine and Coastal Research, East China Normal
8 University, Shanghai 200241, China

9 ^b IHE Delft, Delft, the Netherlands

10 ^c Deltares, Delft, the Netherlands

11 ^d School of Ocean and Earth Sciences, University of Southampton,
12 Southampton, UK

13 ^e Faculty of Civil Engineering and Geosciences, Delft University of Technology,
14 Delft, the Netherlands

15

16 * Corresponding author, E-mail: lcguo@sklec.ecnu.edu.cn

17

18 **Highlights**

19 1. Lateral expansion to low-lying floodplains alleviates the drowning effect of
20 SLR in long tidal basins.

21

22 2. Hypsometry changes under SLR and lateral expansion enhance ebb
23 dominance and sediment export from the basin.

24

25 3. Tidal flats in an unconstrained tidal basin may survive low but not high SLR at
26 the centennial time scale.

27

28 **Abstract**

29 Global climate changes have accelerated sea-level rise (SLR), which
30 exacerbates the risks of coastal flooding and erosion. It is of practical interest to
31 understand the long-term hydro-morphodynamic adaptation of coastal systems
32 to SLR at a century time scale. In this work we use a numerical model to explore
33 morphodynamic evolution of a schematized tidal basin in response to SLR of
34 0.25 to 2.0 m over 100 years with special emphasis on the impact of lateral
35 basin expansion. Starting from a sloped initial bed, morphodynamic
36 development of the system leads to the formation of alternating bars and
37 meandering channels inside the tidal basin and an ebb-tidal delta extending
38 seaward from the basin. Imposing rising sea level causes progressive
39 inundation of the low-lying floodplains, found along the basin margins, inducing
40 an increase in basin plain area and tidal prism, as well as intertidal area and
41 storage volume. Although the overall channel-shoal structure persists under
42 SLR, lateral basin expansion alters the basin hypsometry, leading to enhanced
43 sediment export. The newly-submerged floodplains partly erode, supplying
44 sediment to the system for spatial redistribution, hence buffering the impact of
45 SLR. The vertical accretion rate of the tidal flats inside the tidal basin lags
46 behind the rate of SLR. However, lateral shoreline migration under SLR creates
47 new intertidal flats, compensating intertidal flat loss in the original basin. In
48 contrast, a constrained tidal basin without low-lying floodplains is subject to
49 profound drowning and tidal flat losses under SLR. Overall, the model results
50 suggest that a unconstrained tidal system allowing lateral shoreline migration
51 has buffering capacity that alleviating the drowning impact of SLR by evolving
52 new intertidal areas, sediment redistribution and morphodynamic adjustment.
53 These findings suggest that preserving tidal flats located along the margins of
54 tidal basins (instead of reclaiming them) sustains the system's resilience to
55 SLR.

56 **Key words:** Tidal basin; Sea-level rise; Accommodation space;
57 Morphodynamic modeling

58 **1. Introduction**

59 Coastal areas and wetlands provide important habitats for human beings
60 and ecosystems (Craft et al., 2009; Muis et al., 2016). However, rising sea
61 levels are posing a threat to populated or protected areas, leading to coastal
62 erosion, shoreline retreat, loss of salt-marshes, and increasing risk of flooding
63 (Nicholls et al., 1999). The global mean sea-level rise (SLR) rate has been
64 estimated at 1.8 ± 0.1 mm yr⁻¹ between 1880 and 1980 (Douglas, 1991),
65 increasing to 3.4 ± 0.4 mm yr⁻¹ over the interval 1993-2014 (Nerem et al., 2010;
66 Chen et al., 2017). Although local SLR rates vary slightly in different studies
67 (Dangendorf et al., 2017; Frederikse et al., 2020), it is generally accepted that
68 the rate of SLR is globally accelerating and will continue to accelerate in the
69 future (IPCC, 2014; Chen et al., 2017). It has become a worldwide concern that
70 tidal flat accretion in estuaries and coasts may not be able to keep pace with an
71 accelerated rate of SLR in the coming century. This results in submergence and
72 loss of tidal flats and salt-marshes and associated important habitats and
73 ecosystems (Craft et al., 2009; Kirwan and Megonigal, 2013; Valiela et al.,
74 2018), such as in the Wadden Sea (van Wijnen and Bakker, 2001; Wang et al.,
75 2018; Lodder et al., 2019), San Francisco Bay (Takekawa et al., 2013), and the
76 Mississippi River delta (Blum and Roberts, 2009). Global estimates suggest
77 that 40-90% of coastal wetlands may be lost by the end of the 21st century even
78 when considering marsh accretion and expansion (Ganju et al., 2017; Valiela et
79 al., 2018). The decline in river-borne sediment supply and land subsidence may
80 further accelerate the coastal wetland loss (Syvitski et al., 2009).

81 There is an ongoing debate about the likely impact of an accelerating rate of
82 SLR on estuaries and deltas in the forthcoming century, which is the period of
83 most relevance for present coastal management and planning. In
84 river-dominated deltas, SLR causes delta submergence, shoreline recession
85 and changes in habitat depending on the availability of fluvial sediment and the
86 rate of SLR (van de Lageweg and Slangen, 2017). Differing from open coasts
87 and river deltas, the impact of SLR on tidal basins and estuaries tends to be

88 more complicated because of the non-linear behavior of tidal wave propagation,
89 the interactions between basin geometry and tidal flats, and large-scale
90 estuarine morphodynamic adjustment and feedback mechanism in response to
91 SLR (Du et al., 2018; Lodder et al., 2019). Furthermore, whilst marine
92 transgression on the open coast is invariably normal to the shoreline, the
93 changes in an estuary are more 3-dimensional. For clarity, we consider
94 changes along the axis (thalweg) of the estuary to be landward, for example, if
95 the tidal limit extends further inland. In contrast, lateral changes are those that
96 are normal to the axis or cross-shore, such as erosion of the shoreline which
97 causes a lateral expansion of the estuary.

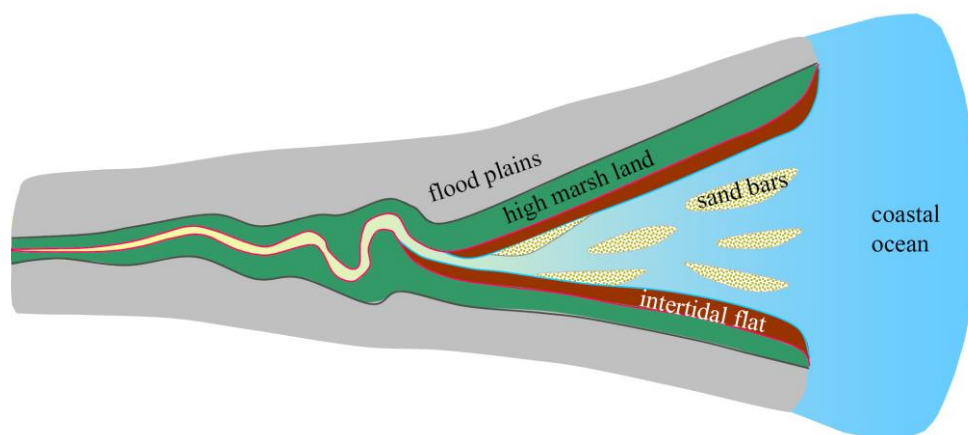
98 Many previous studies have documented changes in tidal wave
99 propagation and hydrodynamics when imposing a higher mean sea level on a
100 fixed morphology (Friedrichs et al., 1990; Wolanski and Chappel, 1996; Du et
101 al., 2018; Talke and Jay, 2020). These studies have stressed the importance of
102 tidal basin planform variations under different water levels and consequent
103 impacts on tidal wave propagation and sediment transport. Others have
104 examined the large-scale response of flats and channels using aggregated
105 models (van Goor et al., 2013; Townend et al., 2016). Examining the likely
106 response, whilst taking account of the redistribution of sediments and the
107 potential changes in morphology, has received far less attention. Schuerch et
108 al. (2018) estimated that 0-30% of the global coastal wetland might be lost as
109 to 2100 provided that sediment supply remains at present levels and no
110 constraints on shoreline migration. This estimated loss is smaller than previous
111 predictions, because of the assumed possible inland expansion, where new
112 wetlands are created. Ladd et al. (2019) and Mariotti and Carr (2014) also
113 stressed that sediment from the lateral erosion of tidal flats might provide
114 sources for vertical accretion. These studies emphasize how tidal systems are
115 able to adjust their own morphology as part of the dynamic response to SLR.
116 They imply that the fate of a tidal system to be drowned or not, depends on its
117 ability to accrete vertically at rates equal to or larger than SLR, and/or to

118 migrate inland at rates faster than shoreline erosion. However, the
119 mechanisms and modes of morphological adjustment that would enable tidal
120 basins to adapt to SLR at the decade to century time scales, when considering
121 both vertical accretion and horizontal migration, are not yet clear. The main
122 evidence for possible mechanisms relies on studies of shoreline retreat and
123 system transgression from sedimentary stratigraphic studies over historic and
124 geological time scales (Allen, 1990; Townend and Pethick, 2002; Dalrymple et
125 al., 2006).

126 Large-scale morphodynamic modeling is a powerful tool in exploring the
127 impact of SLR on estuarine and coastal morphodynamics at the decade to
128 century time scales. Modeling approaches range from highly schematized
129 box-models (e.g., Rossington et al., 2007) to case studies including complex
130 process interactions (e.g., Van der Wegen, 2013). Based on an aggregated
131 approach considering morphological equilibrium concepts (Van Goor et al.,
132 2003; Wang et al., 2018; Lodder et al., 2019), it was suggested that a tidal
133 inlet-basin system, like those in the Dutch Wadden Sea, can survive SLR up to
134 a rate of 15 mm yr⁻¹ owing to the sediment import from ebb-tidal deltas. In
135 contrast, process-based models take complex process descriptions as a
136 starting point. This type of model has a high spatial and temporal resolution but
137 is computationally more expensive than an aggregated approach. The
138 morphodynamic modeling approach has been applied to schematized tidal
139 lagoons and estuaries (Dissanayake et al., 2012; Van Maanen et al., 2013;
140 Van der Wegen, 2013) and also to actual estuaries and tidal basins, such as
141 the sub-embayments of San Francisco Bay (Ganju and Schoellhamer, 2010;
142 Elmilady et al., 2019; Zhang et al., 2020) and the Western Scheldt Estuary
143 (Dam et al., 2013). Most of the past studies documented that intertidal flats in
144 tidal lagoons and estuaries are prone to drown under an accelerating rate of
145 SLR (van der Wegen, 2013; van der Wegen et al., 2016; van de Lageweg and
146 Slangen, 2017; Elmilady et al., 2019).

147 The above-mentioned modeling studies highlight the morphodynamic

148 sensitivity to SLR rates and the high probability of drowning of tidal basins
149 under enhanced rates of SLR scenarios. An important yet under-explored
150 aspect of estuarine adaptation to SLR is the presence of lateral migration of
151 the estuary shoreline, leading to an expansion of plan area under rising sea
152 levels and its subsequent impact on tidal dynamics and morphodynamic
153 evolution. Many tidal basins and estuaries worldwide have a convergent
154 planform and are fringed by large areas of low-lying lands in the lower reaches,
155 which are currently just above high water (see Figures 1 and S1 in the
156 Supporting Information; Dalrymple and Choi, 2007; Bamunawala et al., 2020).
157 Moreover, the low relief of coastal plain tidal basins and estuaries implies that
158 a relatively small increase in mean sea level can lead to a large increase in
159 intertidal area (Kirby, 2000; Friedrichs, 2011). This will have an impact on tidal
160 propagation, subtidal flow and salinity distribution, sediment transport and
161 associated morphodynamic adaptations. Lateral expansion under SLR
162 potentially allows the survival of intertidal flats and marsh systems. Sustainable
163 coastal management strategies, e.g., by introducing more flexible flood
164 protection schemes, could be better developed if there is more knowledge on
165 the benefit of preserving low-lying lands. Therefore, it would be of substantial
166 value for coastal management to understand the degree to which large-scale
167 estuarine morphodynamics adapt to SLR of different rates.



168
169 **Figure 1.** A conceptual diagram of a tide-dominated estuary with mid-channel
170 sand bars, flanked tidal flats and marsh land, and low-lying floodplains,

171 modified from Dalrymple and Choi (2007).

172

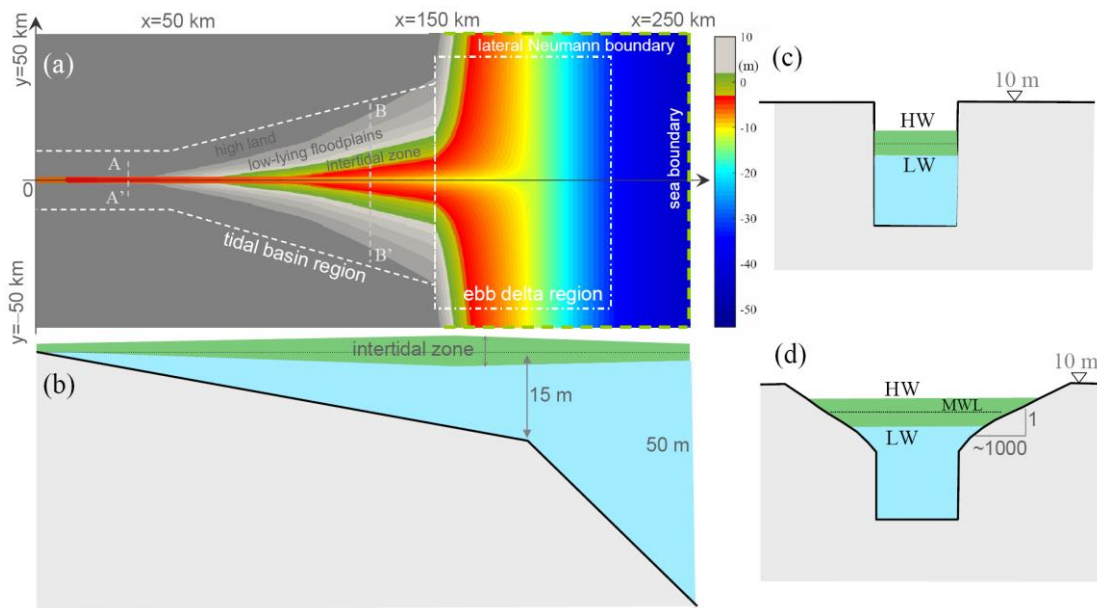
173 The objective of this work is to explore the morphodynamic impact of SLR
174 on a long tidal basin at the centennial time scale when considering the
175 possibility of lateral expansion by using a process-based numerical modeling
176 approach. We first outline the modeling method and settings before presenting
177 the model results in terms of morphological evolution, tidal dynamics and net
178 sediment transport. We then assess the impact of SLR and the implications for
179 estuary management.

180

181 **2. Method**

182 We construct a 2D model of a schematized tidal basin based on the
183 Delft3D software (Lesser et al., 2004) which is a process-based model widely
184 used in modeling estuarine and coastal morphodynamics (see e.g., van der
185 Wegen, 2013; Guo et al., 2015). The model domain is 250 km long and 100 km
186 wide. Longitudinally, the first 150 km is prescribed as a long tidal basin which
187 meets an open coastal ocean extending 100 km offshore (Figure 2a). The tidal
188 basin width at the mean sea level increases from 1 km at the landward end
189 ($x=0$) to 15 km at the mouth section ($x=150$ km), with an initially funnel-shaped
190 planform (Figure 2a). The width convergence length is approximately 270 km
191 (Table 1). The model mesh has a high resolution of 50 m cell size along the
192 tidal basin and around the mouth regions to resolve the channels and shoals
193 formed therein, while the cell size increases slowly to 200 m towards the
194 seaward boundary where morphodynamic changes remain limited. The main
195 channel of the tidal basin has a linearly sloping bed from 0 m at the landward
196 end to 15 m at the mouth section, and further deepens to 50 m at the seaward
197 boundary 100 km offshore (Figure 2b). The initial cross-section profile
198 combines a U-shape in the more landward reach ($x=0$ to $x=50$ km, Figure 2c)
199 and a concave inter- and supra-tidal flat profile in the seaward reach ($x=50$ km
200 to $x=150$ km, Figure 2d). The transverse inter-tidal flat slope is 1/500-1/1500

201 on average in the lower basin, which is close to the mean value observed in
 202 actual estuaries (Le Hir et al., 2000). The concave tidal flat shape is chosen to
 203 be consistent with the fact that tidal flats are more broadly present in the highly
 204 convergent regions of tidal basins and estuaries close to the coasts (Dalrymple
 205 and Choi, 2007) and that tidal flats under tidal forcing controls and with minor
 206 wave influence are more likely to develop concave profiles (Kirby, 2000;
 207 Friedrichs, 2011).



208
 209 **Figure 2.** Sketches of the schematized model domain setting in distorted
 210 space scales: (a) the planform of the tidal basin with division between the inner
 211 basin and the outer delta regions, (b) a side view of the main channel and
 212 initial bed profile, and (c, d) cross-section profiles of A-A' and B-B', respectively.
 213 The green shading indicates the inter-tidal zone. Both the bank and the bed
 214 are erodible. The dashed and dash-dotted boxes in panel (a) indicate the
 215 regions of tidal basin and the ebb delta, respectively.

216

217 **Table 1.** Model parameter settings based on the Delft3D software

Property	Parameter
domain size	(150 +100) km*100 km
cell size	50-200 m
initial channel bed slope	0 m to 15 m
width convergence	convergence length L_b of 270 km (using

	$B=B_0e^{-Lb/x}$
lateral flat slope	1/500~1/1500
bed roughness	uniform Chézy 65 m ^{1/2} /s
horizontal viscosity	1 m ² /s
tidal amplitude	1.5 m at the sea side boundary
sediment	sand of 150 μm in median size
sediment transport formula	Engelund and Hansen (1967)
hydrodynamic time step	60 seconds
hydrodynamic run time	5 years + 1 year
morphological factor	100
morphodynamic time	500 years + 100 years
dry bed erosion parameter	100%
lateral bed slope factor (alfaBn)	10

218

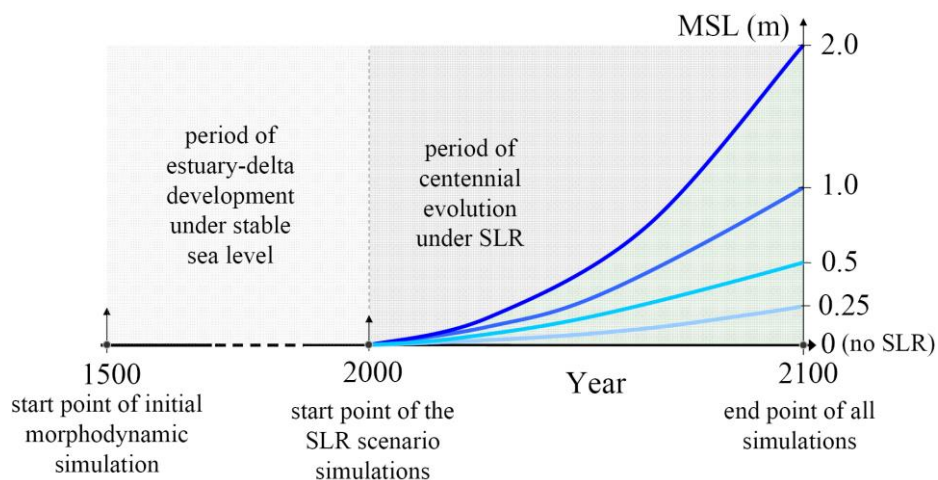
219 The tidal basin is driven by tides with no river flow and fluvial sediment
220 supply and excludes wave impact and density difference effects. For reasons
221 of simplicity, an astronomical semi-diurnal M₂ tide with amplitude of 1.5 m is
222 imposed at the seaward boundary. Other tidal constituents such as S₂ and M₄
223 are not considered although including them would increase tidal range and
224 high-water level, which may induce more inundation. It is assumed that the
225 tides at the seaward boundary will not change much under SLR. Tidal
226 propagation into the tidal basin does, however, adapt in response to
227 morphological changes. The two lateral boundaries of sea domain are
228 prescribed as Neumann boundary conditions, following Roelvink and Walstra
229 (2004), with no water level gradient in the direction normal to the lateral
230 boundaries. The high land of the tidal basin domain (the dark shade region in
231 Figure 2a) has an elevation of 10 m (above mean sea level) and is not
232 inundated even at high tide, hence free-slip boundaries are imposed there. A
233 uniform friction of Chézy coefficient 65 m^{1/2}/s is used. Sediment transport is
234 prescribed by one single sand fraction (a median grain size of 150 μm) treated
235 as total load transport by the Engelund and Hansen (1967) formula.
236 Morphodynamic development is accelerated by using a morphological factor
237 approach based on the Exner equation (Roelvink and Reniers, 2011). Similar
238 to Guo et al. (2015), a morphological factor of 100 is used to accelerate bed

239 level update in this work.

240 To enable channel migration and dry land erosion, the function of dry bed
241 erosion is activated. Dry and wet cells are classified by a depth threshold of 0.1
242 m (Deltares, 2011). In addition, the dry cells adjacent to a wet cell are assumed
243 to be erodible and the erosion volume of the dry cell is prescribed by a
244 user-defined fraction (0-100%) of the erosion in the wet cell. Previous
245 modeling studies considering dry cell erosion show that a fraction of 100% is
246 suitable to reproduce sand bar erosion and channel migration (van der Wegen
247 and Roelvink, 2008; Guo et al., 2015), and is used in this study as well.
248 Moreover, bed slope effects on the sediment transport are considered using
249 the Ikeda (1982) and Bagnold (1986) methods, with lateral and longitudinal
250 bed slope adjustment factors of 5 and 10, respectively (Table 1). The
251 secondary flow impact is considered, whereas Coriolis effect, land subsidence,
252 uplift, and vegetation controls are not considered at this moment. Overall, the
253 size and the forcing conditions of the schematized model are inspired by the
254 conditions of the tide-dominated North Branch of the Changjiang Estuary (Guo
255 et al., 2021). As it is challenging to reproduce the historical centennial
256 morphodynamic evolution of the North Branch with acceptable accuracy, in this
257 study we have adopted a schematized representation to gain insight into the
258 generic response of this specific class of tidal systems.

259 For this study, we first run a morphodynamic simulation for 500 years
260 during which channels and shoals take shape inside the tidal basin and
261 sediment deposition in the mouth builds up an ebb delta. The morphology at
262 the end of 500 years (see Figure 4a) is then used as the initial condition for
263 sensitivity simulations considering SLR. We continue the morphodynamic
264 simulation for another 100 years without SLR, as a reference scenario. It is
265 projected that the most likely SLR by 2100 is some 0.44 m (ranging from
266 0.26-0.61 m), 0.53 m (0.36-0.71 m), and 0.74 m (0.52-0.98 m) according to the
267 Representative Concentration Pathway (RCP) scenarios 2.6, 4.5 and 8.5,
268 respectively, while a high-end scenario suggests a rise of 2-2.5 m (Church et

269 al., 2013). Accordingly, in this study four sensitivity scenarios are defined by
 270 imposing SLR of 0.25, 0.5, 1.0, and 2.0 m over 100 years as an exponential
 271 increase (Figure 3), which equates to mean SLR rates of 2.5, 5, 10, and 20
 272 mm yr⁻¹, respectively. To assist comparison of the situation without lateral
 273 expansion, we also ran extra simulations by imposing thin dams along the high
 274 water shorelines, as defined by the model results at the end of the initial
 275 500-year simulation. This has the effect of removing the low-lying floodplains,
 276 with elevations above the high water, from the model domain, so that they are
 277 not flooded in the following 100-year simulations even under SLR,
 278 representing a diked and constrained tidal basin in which lateral expansion is
 279 not allowed (see section 4.1). Selected morphodynamic properties are
 280 compared with the reference scenario to highlight the impact of SLR, including
 281 the erosion and deposition pattern, the variations of inter-tidal flat area and
 282 storage volume, and tidal wave dynamics and tidally-averaged sediment
 283 transport.



284

285 **Figure 3.** A sketch showing mean sea level changes in the morphodynamic
 286 time framework considering different rates of SLR. The first 500 years are
 287 squeezed in time scale as indicated by the dashed line.

288

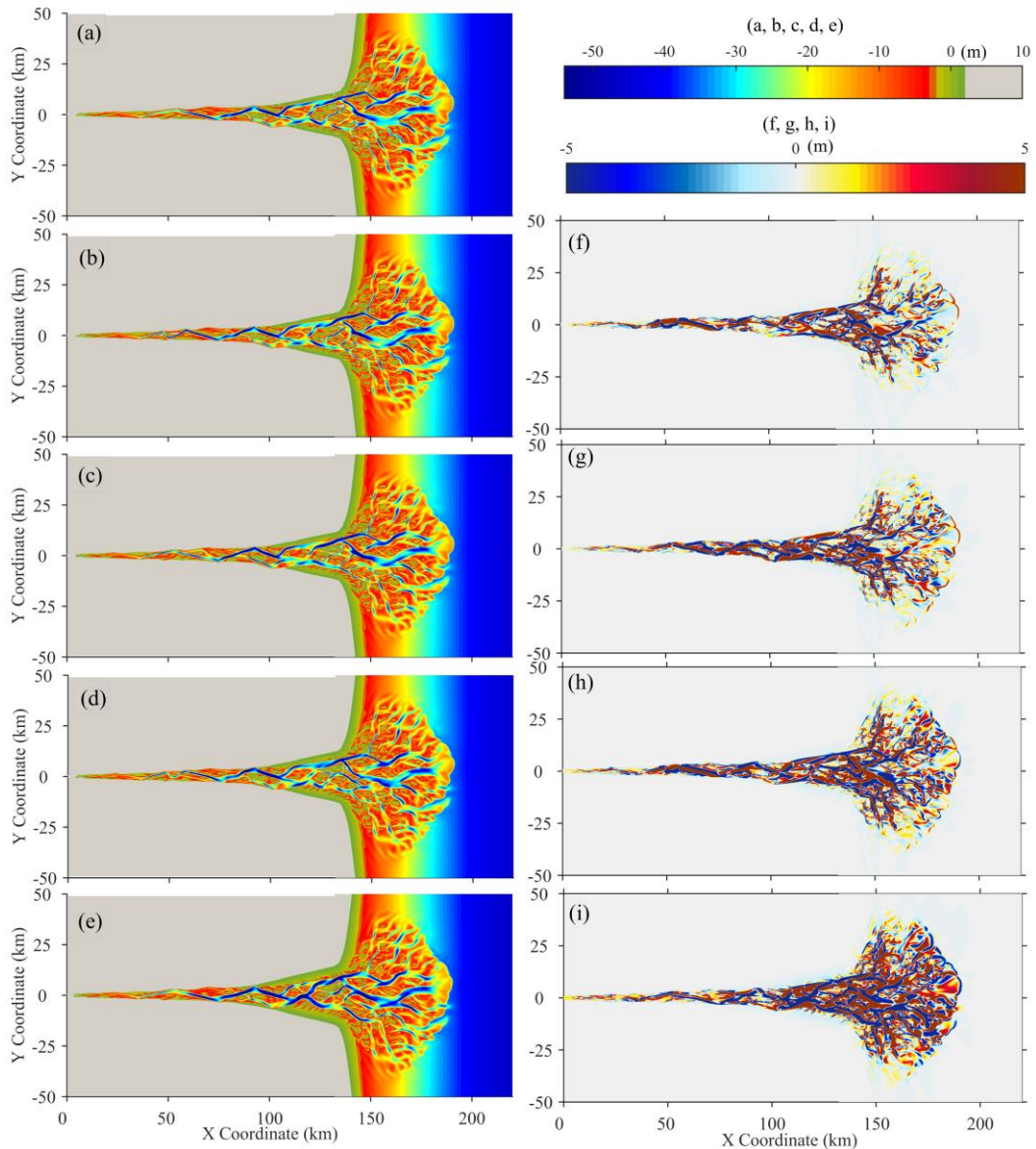
289 3. Model results

290 3.1 Morphodynamic evolution

291 The initial 500-year morphodynamic simulation leads to the development

292 of meandering channels and shoal systems inside the tidal basin and the
293 formation of an ebb-tidal delta with bifurcating channels seaward of the basin
294 mouth. Given no external sediment sources, erosion of the channel bed and
295 channel banks inside the tidal basin and spatial redistribution of the sediment
296 initiates the morphodynamic changes. The ebb delta builds up rapidly by
297 sediment export from the basin that leads to continuous delta progradation.
298 The morphodynamic development gradually slows down after 500 years when
299 a matured channel-shoal structure takes shape and the change rates decline
300 (see supplementary animation A1). However, it is noteworthy that a static
301 morphodynamic equilibrium might have not been reached, according to the
302 classification of Zhou et al. (2017).

303 The morphology at the end of 500 morphodynamic years is then used as
304 the initial bathymetry of the 100-year simulations considering SLR (see
305 supplementary animation A2). Although the overall channel-shoal pattern is
306 sustained in the SLR scenarios (Figures 4a-e), channel migration and sand bar
307 movement continue inside the tidal basin, leading to strong erosion and
308 deposition (Figure 4f-i). Under rising sea-level conditions, the shoreline within
309 the tidal basin laterally migrates across the low-lying land (Figures 5 and S3),
310 and the lateral expansion is more significant under higher SLR. For instance,
311 the maximum lateral migration distance is up to 5 km in the SLR 2.0 scenario.
312 Other than the adjustment of channels and shoals in the SLR scenarios, the
313 newly-submerged floodplains undergo slight erosion (Figure 5). On the
314 seaward side, the ebb delta continues to grow over the 100 years in all
315 scenarios (see Figure S2). The ebb delta progradation, however, is smaller in
316 magnitude in the SLR scenarios compared with the reference case, as
317 indicated by the seaward extent of the ebb delta shoreline (Figures 4f-i).
318 Higher SLR causes more land inundation in the tidal basin and less
319 progradation of the ebb delta.

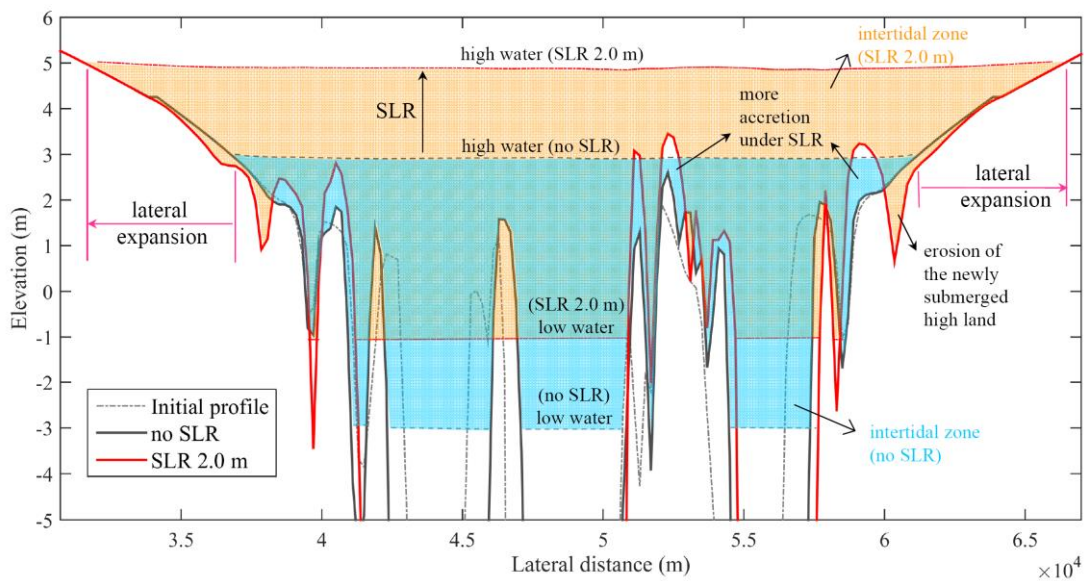


320

321 **Figure 4.** The morphology after 100 years considering (a) no SLR, SLR of (b)
 322 0.25 m, (c) 0.5 m, (d) 1.0 m, and (e) 2.0 m, and accordingly bathymetry
 323 differences between the reference scenario and the scenarios with SLR of (f)
 324 0.25 m, (g) 0.5 m, (h) 1.0 m, and (i) 2.0 m. The green shading in panels (a) to
 325 (e) roughly indicates inter-tidal zone. The dashed lines in panels (f) to (i)
 326 indicate the 2 m elevation contour in the reference scenario and the solid lines
 327 are the 2 m elevation contour in the SLR scenarios. Positive values in panels (f)
 328 to (i) indicate accretion while negative values indicate erosion in the SLR
 329 scenarios compared to the reference case. The bed elevation in panels (b) to
 330 (e) is referenced to the raised mean sea levels in the SLR scenarios, with the

331 elevation of MSL raised by 0.25 m, 0.5 m, 1.0 m and 2.0 m, respectively.

332 The plan area and bankfull width (at high water) of the tidal basin increases
333 with rising sea-levels (see Figure S3). As lateral expansion is more significant
334 in the seaward part of the tidal basin owing to the prescribed tidal flat profile,
335 the width convergence rate becomes slightly larger under SLR (Figure S3).
336 Moreover, the cross-sectionally averaged bed levels largely increase in
337 elevation with SLR (see Figure S4), owing to larger lateral expansion and
338 accretion on the shoals than offsetting the extent of channel deepening.
339 However, the cross-sectionally averaged water depth, which was calculated as
340 the ratio of cross-sectional area to cross-sectional width at the surface, may
341 decrease in the SLR scenarios, because there is a greater increase in
342 cross-sectional width than in cross-sectional area.



343
344 **Figure 5.** Changes of a cross-section profile at $x=130$ km (the deeper part of
345 the channel segment is not shown) and associated high water and low water
346 changes in the reference run and 2.0 m SLR scenario including lateral
347 expansion and extra erosion of the newly-submerged inland zone under SLR.

348 349 **3.2 Tidal dynamics and net sediment export**

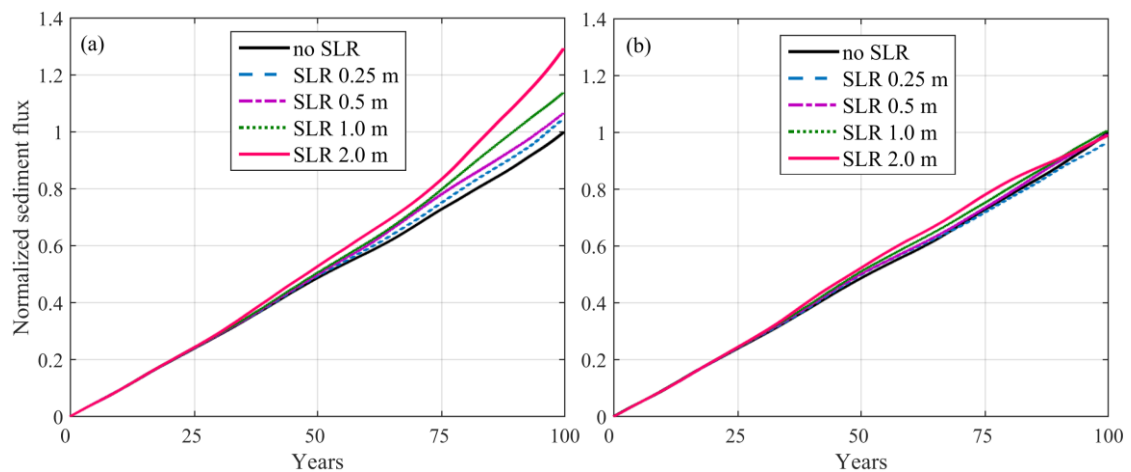
350 At the beginning of the 100-year sensitivity simulations, the amplitudes of
351 the tides traveling into the tidal basin are amplified because the effect of width

352 convergence is stronger than frictional damping. The tidal amplitude increases
353 slowly from 1.5 m at the seaward boundary to 2 m at the basin mouth, and
354 further to 3.8 m inside the estuary before reducing to zero at the landward
355 boundary (see Figure S5). In addition, significant overtides like M_4 (up to 0.75
356 m in amplitude) are generated internally. The tidal wave deformation exhibits
357 longer falling tide than rising tide, and the peak ebb currents are stronger than
358 the flood currents (see Figure S6), suggesting overall ebb dominance of sand
359 transport within the tidal basin. The stronger peak ebb currents are ascribed to
360 the combined impact of a seaward residual current induced by Stokes return
361 flow and the hydraulic storage effect of the intertidal flats which is likely to
362 enhance ebb currents. The former results in a seaward mean water gradient,
363 with the mean water level elevated by up to 0.5 m at the landward end (see
364 Figure S4), and predominantly seaward residual currents (see Figure S7).

365 The amplitudes of the tides are slightly more amplified by the end of the
366 100-year simulation for the reference scenario because of the deepening of
367 the main channel (Figure S5). This also holds true for all other scenarios, while
368 the tides in the 2.0 m SLR scenario are slightly more amplified compared with
369 the reference case. Changes in the internally generated M_4 tide are small
370 under SLR. Overall, the changes in tidal range caused by SLR are insignificant
371 in this study. However, as the surface plan area and cross-section area
372 increase with rising sea levels, the tidal prism of the tidal basin increases with
373 SLR, e.g., by up to 27% in the 2.0 m SLR scenario compared with the
374 reference case (see Figure S9). This increase in tidal prism is mainly ascribed
375 to larger surface area under higher mean sea levels, rather than any increase
376 in tidal range.

377 The tidal changes lead to sediment transport adjustment. In the reference
378 scenario, the net sediment transport flux at the mouth section of the tidal basin,
379 i.e., the interface between the inner basin and outer delta at $x=150$ km, is
380 persistently seaward (see Figure 2a), indicating continuous sediment export
381 from the tidal basin towards the outer ebb delta (Figure 6a). This is in line with

382 the ebb dominance already noted. Other than the landward net sediment
 383 transport in the utmost upstream regions (which explains the accretion and
 384 shoaling therein), the tidally-averaged sediment transport remains
 385 predominantly seaward while its magnitude increases in the seaward direction
 386 (see Figure S8). Moreover, SLR enhances the seaward sediment export rate
 387 and a higher SLR leads to more sediment export (Figure 6a). The impact of
 388 SLR on the sediment export from the constrained basin remains very limited
 389 (Figure 6b). The impact of SLR is not significant in the first 50 years and is
 390 more pronounced when the mean sea level becomes higher. Specifically, the
 391 cumulated sediment export over 100 years is approximately 25% larger under
 392 a SLR of 2.0 m compared with the reference scenario (Figure 6a).



393

394 **Figure 6.** The cumulative sediment flux at the mouth section over the 100
 395 years which are normalized by the cumulated flux in the no SLR scenario: (a)
 396 unconstrained tidal basin with low-lying lands, and (b) constrained tidal basin
 397 in which expansion to low-lying land is not allowed.

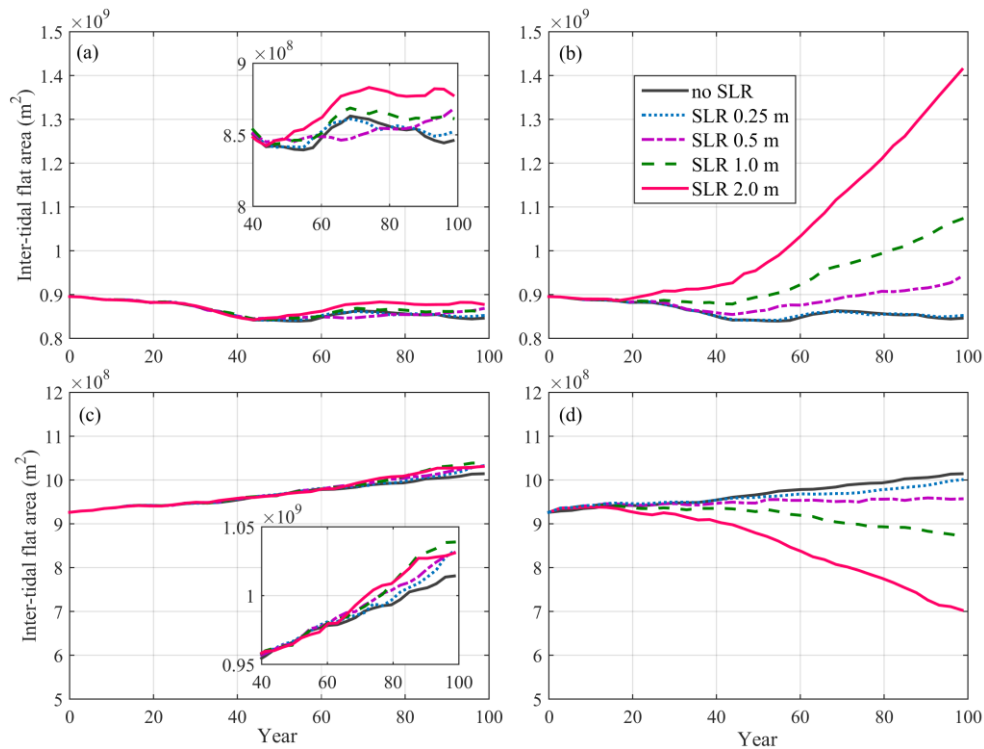
398

399 3.3 Tidal flat evolution

400 In order to check whether the intertidal flats would survive SLR, we
 401 calculate the intertidal flat area based on the integrated areas of the cells with
 402 elevation between high water and low water envelopes. To reveal the effect of
 403 vertical accretion of the previously present tidal flats and the effect of lateral
 404 expansion under SLR, two types of intertidal flat areas are calculated: (1) using

405 a fixed frame for all bathymetries over the 100 years, with the initial high and
406 low water envelopes as the fixed frame of reference and computing the
407 intertidal area between the two surfaces, and (2) using a moving frame over
408 the 100 years, with gradually adapted high and low water envelopes in
409 response to SLR as a moving frame of reference to compute the intertidal area
410 (see Figure S10). Changes in the former intertidal areas mainly reflect the net
411 accretion or erosion of the initially present tidal flats, while the latter indicates
412 the combined effect of vertical tidal flat accretion, lateral shoreline expansion
413 and changing mean sea levels. As the vertical tidal flat accretion is relatively
414 small over the 100 years (see Figure 5), the differences between the two
415 calculations thus predominantly reflect the impact of lateral expansion under
416 SLR.

417 In the fixed tidal frame, the intertidal flat areas in the tidal basin largely
418 decreases over time in the reference scenario, as a result of continued
419 sediment loss to the sea. For the SLR scenarios, the reduction in intertidal
420 area is slightly smaller compared with the reference case (Figures 7a), as
421 indicated by the vertical flat accretion under SLR (see Figure 5). It suggests
422 that the intertidal flats inside the tidal basin are less eroded under SLR, which
423 is confirmed by a smaller surface area at low water (Figure 8a). However, more
424 sediment export occurs in the SLR scenarios, which is partly ascribed to the
425 enlarged tidal prism (see Figure S9). In contrast, the ebb delta exhibits an
426 increase in intertidal area in the reference scenario due to a net sediment gain,
427 and SLR leads to more accretion over the tidal flats as expected (Figure 7c).

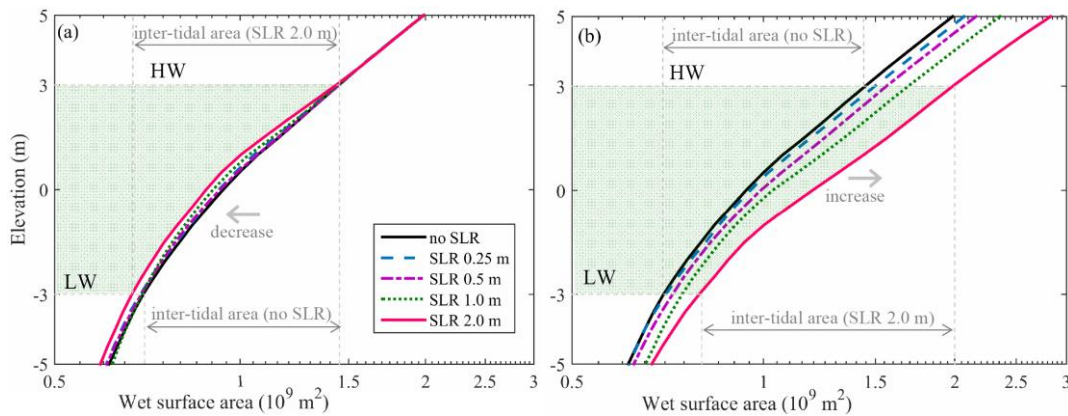


428

429 **Figure 7.** Inter-tidal flat area changes in the tidal basin (a, b) and in the ebb
 430 delta (c, d) with respect to a fixed tidal frame (a, c) and with respect to a
 431 moving frame of reference level following SLR (b, d). The inset plots in (a) and
 432 (c) expand the last 60 years.

433

434 Considering a moving tidal frame, the reduction in intertidal flat areas
 435 becomes much smaller within the tidal basin, while a shift to increase occurs in
 436 the scenarios considering SLR >5 mm yr⁻¹ (Figures 7b and S10). The increase
 437 in intertidal flat areas is much more profound under a SLR of 1.0 and 2.0 m.
 438 The increase in intertidal area inside the tidal basin is predominantly ascribed
 439 to the newly-inundated floodplains that are converted from supra- into
 440 inter-tidal flats. This is also confirmed by a larger increase in surface area at
 441 high water than low water (Figure 8b).



442

443

444

445

446

447

448

449

450

451

452

453

454

455

456

457

458

459

460

461

462

463

464

465

Figure 8. Hypsometry changes (sub-tidal to supra-tidal zones) of the tidal basin in the (a) fixed frame of reference level, where the 0 datum of mean tide level is unchanged, and (b) a moving frame of reference level, where the 0 datum is adjusted to reflect the change in sea level after 100 years.

Similarly, the increase in intertidal flat area in the ebb delta becomes smaller under low SLR and a shift to a decrease occurs in the scenarios with SLR of 1.0 and 2.0 m (Figure 7d). It suggests that the intertidal area in the ebb delta continues to increase under low SLR (albeit at a smaller rate compared with the reference scenario), but the intertidal area decreases in the high SLR scenarios. Overall, the vertical tidal flat accretion rates in the ebb delta lag behind higher SLR rates, despite more sediment supply from the tidal basin.

Detection of the changes in the low (low water to mean water) and high (mean water to high water) intertidal flats separately further demonstrates the influence of lateral expansion. When considering a moving tidal frame, the high intertidal flat areas are overall larger than the low flat areas inside the tidal basin, i.e., the former is approximately twice of the latter at the beginning, because of the concave flat profile shape (Figure 8). The low intertidal areas increase by ~16% over the 100 years in the reference scenario, and the increase becomes more significant in the SLR scenarios (Figure S11a). The high intertidal areas, however, decrease by ~15% in the reference scenario, and a low SLR slows down the decrease whereas a high SLR induces a rapid increase, particularly in the last 50 years (Figure S11b). In contrast, low

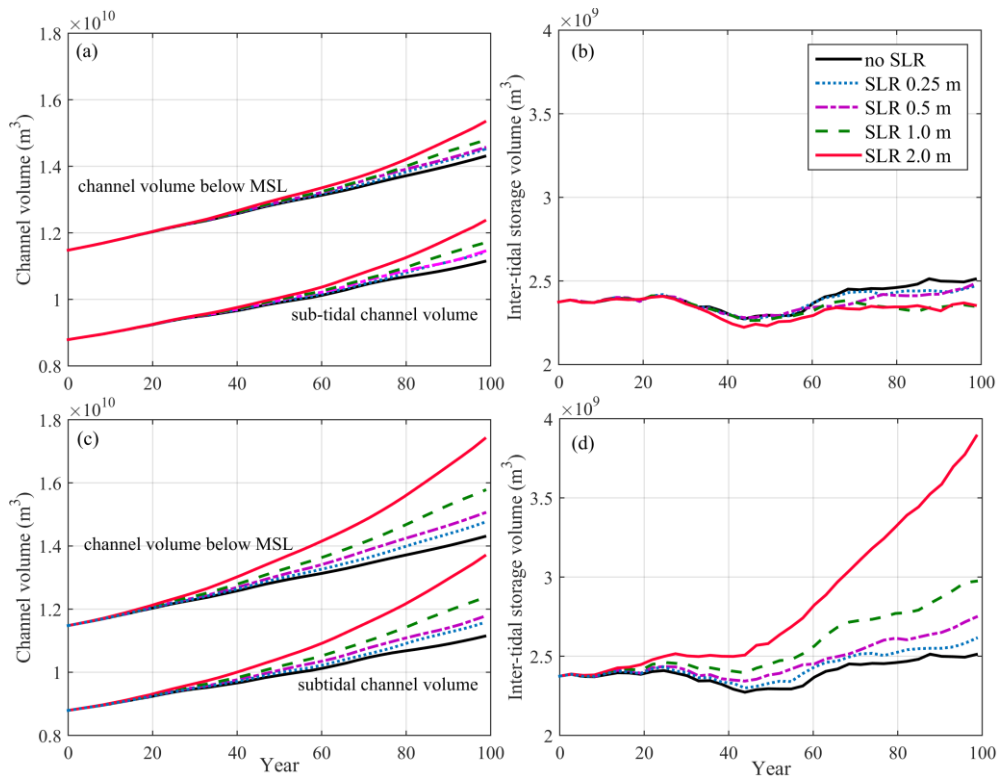
466 intertidal areas are larger than the high flat areas in the ebb delta region
467 (Figure S11c and S11d), suggesting the natural build-up of tidal flats; both the
468 low and high flat areas increase over time in the reference scenario, while SLR
469 induces a shift to decrease, particularly in the high intertidal areas. The
470 decrease in high intertidal areas (Figure S11d) dominates the reduction in the
471 total intertidal areas (Figure 7d) in response to SLR.

472

473 **3.4 Volume changes**

474 Both the channel volumes of the tidal basin below the mean water level
475 and low water increase over time in all scenarios (Figure 9a), which is
476 consistent with the result of net sediment export (see Figure 6). The intertidal
477 storage volume does not show monotonic change, but a temporal decrease
478 during the first 25-45 years, although the intertidal storage at the end of 100
479 years is larger than that at the beginning (Figure 9b). SLR, however, induces a
480 decrease in intertidal volume (evaluated on the fixed frame) compared with the
481 reference scenario. Given that the intertidal area is comparatively larger in the
482 SLR scenarios (see Figure 7a), it suggests that the initially present intertidal
483 zone gains sediment under SLR. Overall, these results indicate that SLR leads
484 to subtidal channel erosion and intertidal accretion in the tidal basin.

485 The calculation on a moving tidal frame demonstrates that the increase in
486 channel volumes is more significant under SLR (Figure 9c). In contrast, the
487 intertidal storage volume increases at a larger rate than the reference scenario
488 (Figure 9d). The differences in the calculation between the fixed and moving
489 frames suggest the role of lateral expansion in modulating the channel-flat
490 morphology as regards to the increase in plan areas, channel volumes, and
491 inter-tidal storage volumes.



492

493 **Figure 9.** Changes of (a, c) channel volumes below mean sea level (MSL) and
 494 low water (subtidal), and (b, d) intertidal storage volumes inside the tidal basin.
 495 The panels (a, b) and (c, d) are the results calculated according to fixed and
 496 moving tidal frames, respectively.

497

498 **4. Discussion**

499 **4.1 Importance of lateral expansion**

500 To indicate the importance of the low-lying land under SLR, we run extra
 501 simulations by removing the low-lying floodplains with elevation above the high
 502 water at the beginning of the SLR scenarios, to represent a constrained tidal
 503 basin. The shorelines within the tidal basin are then fixed and do not migrate
 504 laterally under SLR (see Figure S12). Compared with an unconstrained tidal
 505 basin (with low-lying lands), the tidal prism still increases with rising sea levels
 506 in the constrained basin, but at a smaller rate (see Figure S9b). However, the
 507 sediment flux at the mouth does not increase with SLR compared with the
 508 reference scenario in the constrained basin (see Figure 6b). The intertidal flat
 509 areas decrease at a larger rate compared with the reference scenario, which

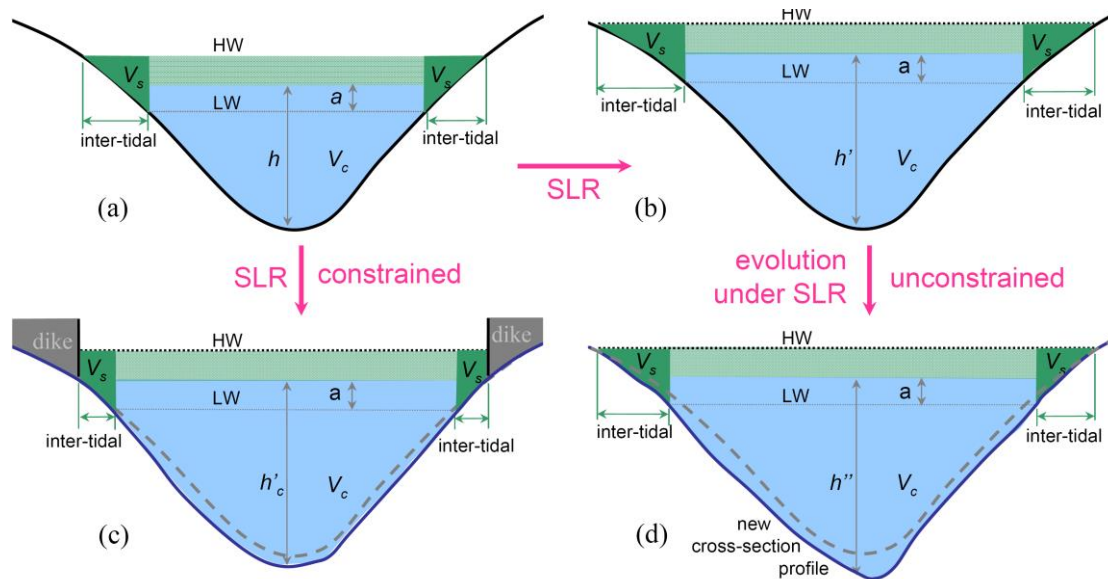
510 contrasts strongly with an increase in the unconstrained basin (see Figure
511 S13). It is because the constrained tidal basin exports sediment and the initially
512 present tidal flats are submerged under SLR, both of which enhance the
513 drowning of the tidal basin and the losses of intertidal flats.

514 The above comparison suggests that the low-lying land flanking the main
515 channel is an important component of the dynamic behavior of the tidal basin
516 by influencing tidal prism, tidal asymmetry and subsequent sediment transport.
517 The hydraulic storage effect of intertidal zones is likely to induce stronger ebb
518 currents, which leads to ebb dominance and sediment export (de Swart and
519 Temmerman, 2009; Robins and Davis, 2010; Ridderinkhof et al., 2014). The
520 ebb dominance of net sediment transport in this study is attributed to the
521 combined influence of the intertidal flat storage effect and a seaward return
522 flow compensating the Stokes drift. The Stokes return flow becomes important
523 in long tidal basins where non-standing waves develop (van der Wegen et al.,
524 2008; Guo et al., 2014). The seaward residual current itself would induce
525 seaward tidally-averaged sediment transport. Furthermore, its interaction with
526 the oscillating tidal currents could drive seaward tidally-averaged sediment
527 transport as well (Guo et al., 2014). Sediment export persists in all simulations,
528 which is probably because static morphodynamic equilibrium has not been
529 reached.

530 In addition, lateral shoreline migration and expansion under SLR creates
531 new tidal flats, which compensate intertidal flat loss owing to drowning of the
532 initially present flats. Moreover, the subsequent changes in basin geometry
533 and hypsometry alter tidal asymmetry and associated sediment export. The
534 SLR-induced change in tidal wave deformation is small as the amplitudes and
535 phases of the principle tide and overtide change marginally. As the depth of the
536 main channel increases under SLR, the magnitude of Stokes return flow would
537 decrease, because it is distributed over a larger water column (Ridderinkhof et
538 al., 2014). However, the intertidal storage volume increases at a larger rate
539 than the increase in channel volume in the SLR scenarios, which leads to a

540 smaller reduction in the intertidal storage volume to channel volume ratio
541 compared to the reference case, even an increase in the SLR 2.0 m scenario
542 (see Figure S14). Such changes suggest enlarged intertidal storage effect
543 under SLR, which would dominate over the other changes and eventually
544 enhance the ebb dominance. Moreover, the tidal prism increases at a larger
545 rate when lateral expansion is allowed, which also benefits larger sediment
546 transport flux. Although more sediment is exported out of the tidal basin under
547 SLR, lateral expansion to low-lying floodplains makes new tidal flats which
548 counteract the drowning impact of SLR.

549 The above discussion implies that allowing lateral expansion changes the
550 system's morphodynamic behavior. An unconstrained tidal basin has a buffer
551 capacity which, to some degree, alleviates the drowning effect of SLR through
552 sediment redistribution within the system, both vertically and horizontally
553 (Figure 10). The tidal basin provides a space for tidal evolution under SLR. The
554 altered tidal asymmetry then plays a role in redistributing sediment and
555 controlling the direction of morphodynamic adaptation. Other than the
556 consequence of a direct tidal flat loss under SLR, the morphodynamic
557 adaptation of unconstrained tidal basins to SLR has larger variability than the
558 situation in open coasts and river deltas, given the dynamic changes in mean
559 water depth, tidal wave propagation, basin hypsometry, sediment redistribution
560 and the morphodynamic feedback mechanism.



561

562 **Figure 10.** Sketches showing the cross-section profile changes under SLR
 563 and consequent morphological evolution: (a) initial condition; (b) under SLR,
 564 and with morphological changes under SLR in (c) constrained and (d)
 565 unconstrained tidal basin. HW and LW indicate high water and low water,
 566 respectively, and V_c and V_s are channel volume below mean sea level and
 567 inter-tidal storage volume, respectively. The dashed lines indicate the new
 568 profiles considering morphodynamic adjustment under SLR.

569

570 4.2 Impact of SLR

571 The morphodynamic modeling results demonstrate some of the likely
 572 impact of SLR on the types of estuaries considered. An increase in channel
 573 width and the areas of shallow tidal flats under SLR might result in a decrease
 574 in tidal amplitude, as tidal amplitude is negatively proportional to channel width
 575 (Jay, 1991). An increase in channel depth implies a smaller friction, which
 576 would increase tidal current velocity and tidal prism. This change would amplify
 577 tidal range in shallow tidal basins and estuaries (van der Wegen and Roelvink,
 578 2008; van der Wegen et al., 2008). In this study, however, the water depth
 579 along the tidal basin is comparably large (>15 m), so that the tidal amplification
 580 is less sensitive to SLR because the fractional change in both resonant
 581 frequency and frictional effect is buffered by the large depth (Talke and Jay,

582 2020).

583 When considering morphodynamic adaptations, SLR causes hypsometry
584 changes by increasing water depth and inducing lateral expansion. The low
585 relief of coastal plain tidal basins and the concave tidal flat profile imply the
586 presence of a larger portion of high tidal flats than low tidal flats. Therefore, a
587 small increase in mean sea level is likely to induce a large change in intertidal
588 areas. The newly inundated low-lying lands under SLR have the potential to
589 erode, which reduces their elevation. Moreover, the initial intertidal flats
590 accrete under SLR but their vertical accretion rate lags behind SLR. For
591 instance, the vertical accretion rate of the tidal flats in the tidal basin is
592 approximately 2.2 mm yr^{-1} larger in the 1.0 m SLR scenario, compared with the
593 reference case, which is smaller than the rate of SLR of 10 mm yr^{-1} (see Figure
594 S15). Hence, although SLR induces more sediment export, the intertidal flat
595 zone inside the tidal basin laterally migrates and the intertidal area does not
596 necessarily shrink.

597 The morphodynamic response of the ebb delta to SLR is similar to that of
598 river-dominated deltas in past studies (van de Lageweg and Slangen, 2017).
599 The exported sediments mainly deposit in the ebb delta front regions, which
600 leads to more delta progradation (horizontal expansion in delta area) than
601 aggradation (vertical increase in elevation) (Figure S7). This is partially
602 because the ebb delta keeps advancing given no waves and alongshore
603 currents that transport the sediment away. The tidal flats over the ebb delta are
604 drowned under SLR although more sediment is available. When taking the
605 tidal basin and ebb delta as a whole into consideration, their total intertidal
606 areas do not decrease owing to the lateral expansion under SLR.

607 The vertical flat accretion rate does not match SLR at the centennial time
608 scale. The impact of SLR is much more significant in the last 50 years owing to
609 a prescribed exponential increase in sea level over time. From this study and
610 previous studies (van der Wegen, 2013), one explanation is that the
611 morphodynamic adaptation occurs at a slower rate than the changes in sea

612 level and associated hydrodynamics. The adaptation time scale of large-scale
613 morphodynamics is very large, possibly longer than 100 years (van der Wegen,
614 2013; Lodder et al., 2019). Note that the morphodynamic time scale of a tidal
615 basin is dependent on system dynamics like tidal strength, accommodation
616 space, and the amounts of sediment being transported during a tidal cycle.
617 Previous studies reported that the morphodynamic time scale is comparably
618 shorter for the Humber Estuary in the UK (e.g., ~40 years) and longer for the
619 Western Scheldt Estuary in the Netherlands (e.g., >100 years) (Jeuken et al.,
620 2003). This time scale difference could influence the morphodynamic behavior
621 in response to long-term changes like nodal tide and sea level (Wang and
622 Townend, 2012). Determination of the morphodynamic time scale of simplified
623 systems can be made by considering basin surface area, channel volume, and
624 sediment concentrations etc. (Kragtwijk et al., 2004; Townend et al., 2016), but
625 it remains technically challenging for complicated systems. Another uncertainty
626 is that the morphodynamic time-scale in the model may not match that of
627 estuaries in nature, due to the use of the morphological acceleration approach
628 and the simplified settings.

629

630 **4.3 Limitations and implications of this study**

631 Interpretation of the findings from the schematized tidal basin should be
632 confined to the forcing and boundary conditions in this study. The tides are
633 very much amplified inside the tidal basin owing to strong channel
634 convergence, with tidal ranges >4.0 m, which represents a macro-tidal
635 environment (Davis, 1964). The strong tides stimulate morphodynamic
636 development and rapid formation of the channel-shoal structure in the initial
637 500 years. In addition, a large tidal range is accompanied by a wide intertidal
638 zone, which serves to highlight the potential impact of SLR on more inundation
639 of low-lying lands. Lateral expansion would be at a smaller rate in meso- or
640 micro-tidal environments, and sediment transport and morphodynamic
641 adjustment rate might be also smaller and slower. Thereby, micro-tidal

642 systems are likely to be more vulnerable to SLR compared with macro-tidal
643 systems.

644 River flow and associated sediment supply are excluded in this modeling
645 study, making the schematized system more like a tidal embayment than an
646 estuary. An extra simulation considering a river discharge of 1,000 m³/s in the
647 same schematized basin exhibits a similar channel-shoal pattern to the
648 tidally-dominated case (not shown). Including a larger river flow would induce a
649 number of more complex dynamic processes, including raised subtidal water
650 levels, enhanced subtidal currents and associated seaward sediment flushing
651 capacity, water stratification and density currents etc. (Guo et al., 2014;
652 Olabarrieta et al., 2018; Zhou et al., 2020). Guo et al. (2014) suggested that
653 even a small river discharge could overrule the role of tides in controlling
654 tidally-averaged sediment transport and reinforce the seaward sediment
655 flushing and inducing basin emptying, while a high river discharge induces
656 more sediment supply and dampens the tide, which probably cause basin
657 infilling. As the sediment export is enhanced by river flow, it becomes more
658 difficult to sort out the control and the impact of basin hypsometry change on
659 sediment flux. Another factor not considered in this study was the impact of
660 SLR in the presence of waves and storms. Waves and associated alongshore
661 currents would remove sediment from the ebb delta and transport them away,
662 which tends to reduce delta progradation. As the mean sea-level rises and the
663 water depth becomes larger, the wave impacts may reach more inland and
664 may alter the tidal flat morphology particularly over the ebb delta front region.
665 Further investigation of the influence of SLR in estuaries considering river flow
666 and riverine sediment supply and wave forcing would provide greater insight.

667 The initial morphology and simplified setting in this study might also
668 influence the findings about the impact of SLR. The physical length of a tidal
669 basin has impact on tidal wave propagation and subsequent morphodynamics,
670 thereby tidal basins of varying lengths and geometry respond to SLR
671 differently (Du et al., 2018). Morphodynamic adaptation to SLR in short tidal

672 basins and lagoons (basin length \ll tidal wave length) can be different from
673 the long tidal basin in this study, given that standing waves and synchronous
674 tides are prone to occur in short basins. For instance, Dissanayake et al. (2012)
675 found enhanced flood dominance and sediment import in a short tidal
676 inlet-basin system under SLR of 2-7 mm yr⁻¹ over 110 years, whereas van
677 Maanen et al. (2013) reported enhanced sediment export in a similar but
678 smaller system under SLR of 2.8-11.2 mm yr⁻¹ over 200 years. The contrasting
679 results are attributed to the size and shape of the tidal basins which affect tidal
680 evolution and tidal asymmetry under SLR. The shape and gradient of the tidal
681 flat profiles affect the system's buffering capacity to SLR. The concave profile
682 shape in this study benefits submergence of low-lying land under SLR. The
683 morphodynamic adaptation of tidal basin to SLR under different cross-section
684 geometry requires site-specific investigation (Friedrichs et al., 1990; Leuven et
685 al., 2019).

686 The net sediment export reproduced in this study may be overestimated
687 because mud transport is excluded. Consideration of both sand and mud
688 transports may induce more complex behavior given different mechanisms in
689 controlling tidally-averaged transport of coarse and fine sediments (Dronkers,
690 1986). For example, the export of sand and import of mud leading to net
691 sediment import are detected in actual estuaries such as the Western Scheldt
692 Estuary (Dam et al., 2007) and the Humber Estuary (Townend and Whitehead,
693 2003). SLR in such systems leads to an increase in accommodation space,
694 which implies that more sediment import is needed as the system seeks to
695 restore equilibrium (Townend et al., 2007; Van der Wegen, 2013; Lodder et al.,
696 2019). Although the model size and forcing conditions in the schematized
697 model were prescribed to be similar to that of the North Branch in the
698 Changjiang Estuary, the modelled channel pattern is more braided and
699 bifurcated compared with the two-channel configuration found in reality. This
700 difference is probably because mud transport, waves and alongshore currents
701 acting on the North Branch were both excluded. Including mud transport might

702 change the sediment export regime depending upon the relative contents of
703 mud and sand, which needs future in-depth study.

704 The initial morphology used in the SLR scenario simulations might have
705 not approached an equilibrium state yet, although the morphological change
706 rate has slowed down. In an ideal case it would be better to model and analyze
707 the SLR impact when a morphodynamic equilibrium is reached, but
708 morphodynamic equilibrium, either a static or dynamic equilibrium, is
709 technically hard to define (Zhou et al., 2017) and may require much longer
710 computation time for such a large-scale system. Van der Wegen (2013) has
711 examined morphodynamic evolution with SLR under different initial
712 bathymetries and found that the overall change in behavior persists, although
713 the change rates are slightly different. This suggests that the interpretation of
714 SLR impact is not unduly influenced by the initial morphology in the model. It
715 may also be because the impact of the initial morphology is no longer
716 morphologically significant, when compared to the sea level perturbation
717 imposed.

718 The model produced morphology maybe also sensitive to other physical
719 settings like the dry cell erosion parameter and the bed slope effect. Extra
720 sensitivity simulations to examine the role of the dry cell erosion parameter
721 suggests slightly smaller lateral shoreline migration rates when the dry cell
722 erosion function is not activated (0%), or with a smaller dry cell erosion
723 parameter of 50%, compared with the results of 100% (see Figure S16).
724 However, the impact on the channel-shoal pattern and the cumulated sediment
725 flux at the mouth section is overall less apparent. It is worth noting that the dry
726 bed erosion function only produces gradual erosion of the dry cells and does
727 capture other lateral processes like bank collapse and cliff formation. The latter
728 needs extra physical processes such as these examined by Zhao et al. (2019).
729 Extra sensitivity simulations considering smaller ($\alpha_{Bn}=5$) and larger
730 ($\alpha_{Bn}=20$) lateral bed slope effect reveals a more significant impact on the
731 morphology. A smaller lateral bed slope effect leads to more braided channel

732 pattern and larger transverse bed slope between the channels and shoals,
733 while a larger lateral bed slope effect flattens the morphology and leads to less
734 tidal flat area (see Figure S17). These sensitivity model results are consistent
735 with the results in Dissanayake et al. (2012) and Baar et al. (2019),
736 demonstrating the necessity to choose a suitable representation of the bed
737 slope effect when modeling long-term and larger-scale alluvial
738 morphodynamics.

739 This study examines the physical processes only, while the potential
740 impact of vegetation on tidal flat accretion is not considered. The vegetated
741 tidal flats tend to have a larger erosion resistance owing to the root-enhanced
742 substrate contexts, which is likely to reduce dry land erosion. In addition,
743 vegetation stimulates salt-marsh accretion compared with bare flats by
744 increasing sediment trapping in the vegetated regions. Moreover,
745 accumulation of underground organic matter in salt-marshes may also help
746 tidal flat accretion (Thorne et al., 2018). There is increasing evidence that
747 considering the ecological impact of the vegetation canopy can increase the
748 resilience of tidal flats and salt-marshes to SLR (Kirwan et al., 2016; Best et al.,
749 2018). The vegetation canopy is also expected to migrate landward to
750 low-lying land in response to SLR if there is space (Enwright et al., 2016). For
751 example, coastal salt-marsh and mangrove migration under SLR has been
752 detected over Holocene and modern time scales (Cohen et al., 2020).
753 Examination of the mutual evolution of the vegetation and morphology is an
754 emerging topic (Murray et al., 2008; Passeri et al., 2015) and merits future
755 study.

756 Although the schematized model is not supposed to represent specific tidal
757 basins or estuaries in nature, the model domain and forcing settings mimic
758 tide-dominated long tidal basins in coastal plains with low relief which can shed
759 light on their morphodynamic behavior in response to SLR. The model results
760 suggest that the tidal flats in the tidal basin-ebb delta system might survive a
761 low SLR over 100 years, while the drowning impact of a high SLR is mitigated

762 by a negative feedback between geometric change, tidal evolution and
763 morphodynamic adjustment, when lateral expansion is possible. It thus
764 highlights the importance of conserving floodplains and wetlands surrounding
765 tidal channels that provide a critical buffering capacity. However, human
766 activities such as tidal flat reclamation, channel dredging, and construction of
767 dikes and jetties to realign navigation channels (Boltt et al., 2006; Zhao et al.,
768 2018) have substantially modified estuarine morphodynamics and constrained
769 the free behavior of tidal basins and estuaries in the past centuries, such as in
770 the Western Scheldt Estuary (Dam et al., 2013; see Figure S1a) and in the
771 North Branch of the Changjiang Estuary (Guo et al., 2021). Constraining tidal
772 systems by constructing extensive dikes and reclaiming low-lying floodplains,
773 wetlands, and intertidal flats may significantly affect tidal propagation and
774 amplification (Pelling et al., 2013; Talke and Jay, 2020) and reduce the
775 systems' resilience to SLR. This confirms the ongoing mindset change in
776 coastal defense and management reflected in the increasing popularity of soft
777 engineering schemes which leave or restore space for nature (Temmerman et
778 al., 2013; Bouma et al., 2014).

779

780 **5. Conclusions**

781 Understanding the impact of SLR on tidal basins and estuaries in the
782 coming 100 years is of practical interest for coastal management and human
783 development. In this work we deployed a numerical model to explore
784 centennial morphodynamic evolution of a schematized tidal basin with broad
785 tidal flats in response to SLR up to a rate of 20 mm yr⁻¹. We find that sediment
786 export at the basin mouth increased with SLR, owing to increased hydraulic
787 storage on the tidal flats, which favors ebb dominance. The intertidal flat areas
788 throughout the tidal basin and ebb delta increase under a low SLR, e.g., 2.5
789 mm yr⁻¹ in this study. The intertidal flat areas still increase in the tidal basin
790 under a higher SLR owing to lateral incursion, which converts sub-aerial
791 floodplains into intertidal flats, while the ebb delta loses intertidal flats although

792 it receives more sediment. The latter is because the vertical flat accretion
793 occurs at a rate smaller than SLR, which is in turn partly because
794 morphodynamic evolution is in essence much slower compared with the
795 changes in mean sea level and tidal hydrodynamic adaptation.

796 The model results suggest that an unconstrained tidal basin can adapt to
797 low SLR and has some resilience to high SLR by creating new flats and
798 redistributing sediment. Although interpretation of the model results can be
799 influenced by the simplified model settings, the findings in this work provide
800 insights into how SLR may affect natural tidal basin with a strong
801 morphodynamic feedback. It clearly demonstrates the importance of
802 conserving low-lying floodplains and wetlands surrounding tidal channels,
803 which could sustain tidal basin systems' buffering capacity in response to SLR.
804 Further work is needed to consider river and wave forcing, mud transport, and
805 coupled biological and morphological evolution.

806

807

808 **Acknowledgements**

809 This work is supported by the project 'Coping with deltas in transition' within
810 the Programme of Strategic Scientific Alliance between China and The
811 Netherlands (PSA), financed by the Ministry of Science and Technology, P.R.
812 China (MOST) (No. 2016YFE0133700) and Royal Netherlands Academy of
813 Arts and Sciences (KNAW) (No. PSA-SA-E-02), and also partly by MOST (No.
814 2017YFE0107400), Natural Science Foundation of China (Nos. 51739005;
815 U2040216; 41876091), and Shanghai Committee of Science and Technology
816 (Nos. 19QA1402900; 20DZ1204700).

817

818

819 **References**

820 Allen J.R.L., 1990. The Severn Estuary of southwest Britain: its retreat under
821 marine transgression, and fine sediment regime. *Sedimentary Geology*

822 66(1-2), 13-28.

823 Bagnold R.A., 1966. An approach to the sediment transport problem from
824 general physics, US Geological Survey Prof. paper 422-I, Washington, USA.

825 Bamunawala J., Dastheib A., Ranasinghe R., van der Spek A., Maskey S.,
826 Murray A.B., Duong T.M., Barnard P.L., Sirisena T.A.J.G., 2020. A holistic
827 modeling approach to project the evolution of inlet-interrupted coastlines
828 over the 21st century. *Frontiers in Marine Science* 7,
829 10.3389/fmars.2020.00542.

830 Baar A.W., Albernaz M.B., van Dijk W.M., Kleinhans M.G., 2019. Critical
831 dependence of morphodynamic models of fluvial and tidal systems on
832 empirical downslope sediment transport. *Nature communications* 10(1),
833 1-12.

834 Belliard J.-P., Temmerman S., Toffolon M., 2017. Ecogeomorphic relations
835 between marsh surface elevation and vegetation properties in a temperate
836 multi-species salt marsh. *Earth Surface Processes and Landforms* 42,
837 855-865.

838 Best U.S.N., van der Wegen M., Dirkstra J., Willemsen P.W.J.M., Borsje B.W.,
839 Roelvink D.J.A., 2018. Do salt marshes survive sea level rise? Modeling
840 wave action, morphodynamics and vegetation dynamics. *Environmental*
841 *Modelling and Software* 109, 152-166.

842 Blum M.D., Roberts H.H., 2009. Drowning of the Mississippi Delta due to
843 insufficient sediment supply and global sea-level rise. *Nature*,
844 doi:10.1038/NGE0553.

845 Bouma T.J., van Belzen J., Balke T., Zhu Z.C., Airoidi L., Blight A.J., Davis A.J.,
846 Galvan C., Hawkins S.J., Hoggart S.P.G., Lara J.L., Losada I.J., Maze M.,
847 Ondiviela B., Skow M.W., Strain E.M., Thompson R.C., Yang S.L., Zanuttigh
848 B., Zhang L.Q., Herman P.M.J., 2014. Identifying knowledge gaps hampering
849 application of intertidal habitats in coastal protection: opportunities & steps to
850 take. *Coastal Engineering* 87, 147-157.

851 Chen X.Y., Zhang X.B., Church J.A., Watson C.S., King M.A., Monselesan D.,

852 Legresy B., Harig C., 2017. The increasing rate of global mean sea-level rise
853 during 1993-2014. *Nature Climate Change*, doi:10.1038/NCLIMATE3325.

854 Church J.A., Clark P.U., Cazenave A., Gregory J.M., Jevrejeva S., Levermann
855 A., Merrifield M.A., Milne G.A., Nerem R.S., Nunn P.D., Payne A.J., Pfeffer
856 W.T., Stammer D. and Unnikrishnan A.S., 2013: Sea Level Change. In:
857 *Climate Change 2013: The Physical Science Basis. Contribution of Working*
858 *Group I to the Fifth Assessment Report of the Intergovernmental Panel on*
859 *Climate Change [Stocker, T.F., D. Qin, G.-K. Plattner, M. Tignor, S.K. Allen, J.*
860 *Boschung, A. Nauels, Y. Xia, V. Bex and P.M. Midgley (eds.)]. Cambridge*
861 *University Press, Cambridge, United Kingdom and New York, NY, USA.*

862 Cohen M.C.L., Figueiredo B.L., Oliveira N.N., Fontes N.A., Franca M.C.,
863 Pessenda L.C.R., de Souza A.V., Macario K., Giannini P.C.F., Bendassoli
864 J.A., Lima P., 2020. Impact of Holocene and modern sea-level changes on
865 estuarine mangroves from northeastern Brazil. *Earth Surface Processes and*
866 *Landform*, doi.org/10.1002/esp.4737.

867 Craft C.B., Clough J., Ehman J., Joye S.B., Park R., Pennings S.C., Guo H,
868 Machmuller M., 2009. Forecasting the effects of accelerated sea level rise on
869 tidal marsh ecosystem services. *Frontiers in Ecology and the Environment* 7,
870 73-78.

871 Dalrymple R.W., Leckie D.A., Tillman R.W., 2006. Incised valleys in time and
872 space. *Society for Sedimentary Geology* 2006, Tulsa, Okla.

873 Dalrymple R.W., Choi K.S., 2007, Morphologic and facies trends through the
874 fluvial-marine transition in tide-dominated depositional systems: A systematic
875 framework for environmental and sequence-stratigraphic interpretation.
876 *Earth Science Reviews* 81, 135–174.

877 Dam G., Bliet A.J., Labeur R.J., Ides S.J., Plancke Y.M.G., 2007. Long-term
878 process-based morphological model of the Western Scheldt Estuary. In:
879 Dohmen-Janssen C.M. and Hulscher J.M.H. (eds.), *Proceedings of the 5th*
880 *IAHR Symposium on River, Coastal and Estuarine Morphodynamics*, doi:
881 10.1201/NOE0415453639-c135

882 Dam G., van der Wegen M., Roelvink D., 2013. Long-term performance of
883 process-based models in estuaries. Proceedings of the Coastal Dynamics
884 Conference, pp. 409-419.

885 Dangendorf S., Marcos M., Woppelmann G., Conrad C.P., Frederikse T., Riva
886 R., 2017. Reassessment of 20th century global mean sea level rise. PNAS
887 114, 5964-5951.

888 Davis J.L., 1964. A morphogenic approach to world shorelines. Zeitschrift fur
889 Geomorphologie 8, 127-142.

890 de Swart H.E., Zimmerman J.T.F., 2009. Morphodynamics of tidal inlet systems,
891 Annual Review of Fluid Mechanics 41, 203–229.

892 Deltares, 2011. User Manual Delft3D-Flow: Simulation of Multi-dimensional
893 Hydrodynamic Flows and Transport Phenomena, Including Sediments,
894 Version 3.15, Deltares, Delft, Netherlands.

895 Dissanayake D.M.P.K., Ranasinghe R., Roelvink J.A., 2012. The
896 morphological response of large tidal inlet/basin systems to relative sea level
897 rise. Climate Change 113(2), 253–276, doi: 10.1007/s10584-012-0402-z.

898 Douglas B.C., 1991. Global sea level rise. Journal of Geophysical Research
899 96(C4), 6981-6992.

900 Dronkers J., 1986. Tidal asymmetry and estuarine morphology. Netherland
901 Journal of Sea Research 20(2/3), 117-131.

902 Du J.B., Shen J., Zhang Y.L.J., Ye F., Liu Z., Wang Z.G., Wang Y.P., Yu X.,
903 Sisson M., Wang H.V., 2018. Tidal responses to sea-level rise in different
904 types of estuaries: the importance of length, bathymetry and geometry.
905 Geophysical Research Letters 45, 227-235.

906 Elmilady H., van der Wegen M., Roelvink D., Jaffe B.E., 2019. Intertidal area
907 disappears under sea level rise: 250 years of morphodynamic modeling in
908 San Pablo Bay, California. Journal of Geophysical Research: Earth Surface
909 124, 38-59.

910 Engelund F., Hansen E., 1967. A Monograph on Sediment Transport in Alluvial
911 Streams, Teknisk-Forlag, Copenhagen.

912 Enwright N.M., Griffith K.T., Osland M.J., 2016. Barrier to and opportunities for
913 landward migration of coastal wetlands with sea-level rise. *Frontiers in*
914 *Ecology and the Environment*

915 Frederikse T., Landerer F., Caron L., Adhikari S., Parkes D., Humphrey V.W.,
916 Dangendorf S., Hogarth P., Zanna L., Cheng L.J., Wu Y.H., 2020. The
917 causes of sea-level rise since 1900. *Nature* 584, 393-397.

918 Friedrichs C.T., 2011. Tidal flat morphodynamics: A synthesis. In: *Treatise on*
919 *Estuarine and Coastal Science, Estuarine and Coastal Geology and*
920 *Geomorphology*, vol. 3, edited by B.W. Flemming and J.D. Hansom, pp.
921 137–170, Elsevier, Amsterdam.

922 Friedrichs C.T., Aubrey D.G., 1988. Non-linear tidal distortion in shallow
923 well-mixed estuaries: A synthesis. *Estuarine Coastal Shelf Science* 27,
924 521–545.

925 Friedrichs C.T., Aubrey D.G., Speer P.E., 1990. Impacts of relative sea-level
926 rise on evolution of shallow estuaries, In: R.T. Cheng (ed.), *Coastal and*
927 *Estuarine Studies*, vol. 38, p.105–120, Residual currents and long-term
928 transport, Springer-Verlag, New York, US.

929 Ganju N.K., Schoellhamer D.H., 2010. Decadal-timescale estuarine
930 geomorphic change under future scenarios of climate and sediment supply.
931 *Estuaries and Coasts* 33, 15–29, doi 10.1007/s12237-009-9244-y.

932 Ganju N.K., Defne Z., Kirwan M.L., Fagherazzi S., D’Alpaos A., Carniello L.
933 2017. Spatially integrative metrics reveal hidden vulnerability of salt
934 marshes. *Nature Communications* 8, 1-7, doi: 10.1038/ncomms14156.

935 Guo L.C., van der Wegen M., Wang Z.B., Roelvink D., He Q., 2015. Long-term,
936 process-based morphodynamic modeling of a fluvio-deltaic system, Part I:
937 the role of river discharge. *Continental Shelf Research* 109, 95-111.

938 Guo L.C., Xie W.M., Xu F., Wang X.Y., Zhu C.Y., Meng Y., Zhang W.G., He Q.,
939 2021. A historical review of sediment export-import shift in the North Branch
940 of Changjiang Estuary. *Earth Surface Processes and Landforms*,
941 <https://doi.org/10.1002/esp.5084>.

942 Ikeda S., 1982. Lateral bed load transport on side slopes. *Journal Hydraulics*
943 *Division, ASCE*, 108(11), 1369–1373.

944 IPCC, 2014. *Impacts, Adaptation, and Vulnerability. Part A: Global and*
945 *Sectoral Aspects. Contribution of Working Group II to the Fifth Assessment*
946 *Report of the Intergovernmental Panel on Climate Change*, Cambridge
947 *University Press*, Cambridge, United Kingdom and New York, NY, USA.

948 Jeuken M.C.J.L., Wang Z.B., Keiller D., Townend I., Liek G.A., 2003.
949 Morphological response of estuaries to nodal tide variations. In *Proceedings*
950 *of the International Conference on Estuaries and Coasts*, Hangzhou, China,
951 p.166-173.

952 Kirby R., 2000. Practical implications of tidal flat shape. *Continental Shelf*
953 *Research* 20, 1061–1077.

954 Kirwan M., Megonigal J.P., 2013. Tidal wetland stability in the face of human
955 impacts and sea-level rise. *Nature* 504, 53-60.

956 Kirwan M., Temmerman S., Keehan E.E., Guntenspergen G.R., Fagherazzi S.,
957 2016. Overestimation of marsh vulnerability sea level rise. *Nature Climate*
958 *Change* 6(3), 253-260.

959 Kragtwijk N.G., Stive M.J.F., Wang Z.B., Zitman T.J., 2004. Morphological
960 response of tidal basins to human interventions. *Coastal Engineering* 51,
961 207-221.

962 Ladd C.J.T., Duggan-Edwards M.F., Bouma T.J., Pages J.F., Skov M.W., 2019.
963 Sediment supply explains long-term and large-scale patterns in saltmarsh
964 lateral expansion and erosion. *Geophysical Research Letters*, doi:
965 10.1029/2019GL083315.

966 Leuven J.R.F.W., Pierik H.J, van der Vegt M., Bouma T.J., Kleinhans M.G.,
967 2019. Sea-level-rise-induced threats depend on the size of tide-influenced
968 estuaries worldwide. *Nature Climate Change*,
969 doi.org/10.1038/s41558-019-0606-4.

970 Le Hir P., Roberts W., Cazaillet O., Christie M., Bassoullet P., Bacher C., 2000.
971 Characterization of intertidal flat hydrodynamics. *Continental Shelf Research*

972 1433-1459.

973 Lesser G.R., Roelvink J.A., Van Kester J.A.T.M., Stelling G.S., 2004.
974 Development and validation of a three-dimensional morphological model.
975 Coastal Engineering 51, 883–915.

976 Lodder Q.J., Wang Z.B., Elias E.P.L., van der Spek A.J.F., de Looff H.,
977 Townend I.H., 2019. Future response of the Wadden Sea tidal basins to
978 relative sea-level rise—an aggregated modelling approach. Water 11 (10),
979 doi: 10.3390/w11102198.

980 Mariotti G., Carr J., 2014. Dual role of salt marsh retreat: long-term loss and
981 short-term resilience. Water Resources Research 50(4), 2963-2974.

982 Muis S., Verlaan M., Winsemius H.C., Aerts J.C.J.H., Ward P.J., 2016. A global
983 reanalysis of storm surge and extreme sea levels. Nature Communications 7,
984 11969, doi.org/10.1038/ncomms11969.

985 Murray A.B., Knaapen M.A.F., Tal M., Kirwan M.L., 2008. Biomorphodynamics:
986 physical-biological feedbacks that shape landscapes. Water Resource
987 Research 44, W11301, doi: 10.1029/2007WR006410.

988 Nerem R.S., Chambers D.P., Choe C., Mitchum G.T., 2010. Estimating mean
989 sea level changes from the TOPEX and Jason altimeter missions. Marine
990 Geodesy 33, 435-446.

991 Nicholls R.J., Hoozemans F.M.J., Marchand M., 1999. Increasing flood risk
992 and wetland losses due to global sea-level-rise: regional and global analyses.
993 Global Environmental Change 9, S69–S87.

994 Olabarrieta M., Geyer W.R., Coco G., Friedrichs C.T., Cao Z., 2018. Effects of
995 density - driven flows on the long - term morphodynamic evolution of funnel
996 - shaped estuaries. Journal of Geophysical Research: Earth Surface 123,
997 2901-2924.

998 Pelling H.E., Green J.A.M., Ward S.L., 2013. Modelling tides and sea-level rise:
999 to flood or not to flood. Ocean Model 63, 21 - 29.

1000 Ridderinkhof W., de Swart H.E., van der Vegt M., Alembregtse N.C., Hoekstra P.,
1001 2014. Geometry of tidal inlet systems: A key factor for the net sediment

1002 transport in tidal inlets. *Journal of Geophysical Research: Oceans* 119 (10),
1003 6988-7006, doi: 10.1002/2014jc010226.

1004 Robins P.E., Davis A.G., 2010. Morphological controls in sandy estuaries: the
1005 influence of tidal flats and bathymetry on sediment transport. *Ocean*
1006 *Dynamics* 60, 503-517.

1007 Roelvink J.A., Walstra D.J., 2004. Keeping it simple by using complex models.
1008 *Advances in Hydro-science and Engineering* 6, 1-11.

1009 Roelvink J.A., Reniers A.J.H.M., 2011. A Guide to Coastal Morphology
1010 Modeling, *Advances in Coastal and Ocean Engineering*, vol. 12, World Sci.
1011 Co., Singapore.

1012 Rossington K., Nicholls R.J., Knaapen M.A.F., Wang Z.B., 2007. Morphological
1013 behaviour of UK estuaries under conditions of accelerating sea level rise,
1014 Dohmen-Janssen C.M. and Hulscher S.J.M.H. (eds.), RCEM2007, River,
1015 Coastal and Estuarine Morphodynamics, Taylor & Francis.

1016 Schuerch M., Spencer T., Temmerman S., Kirwan M., Wolff C., Lincke D.,
1017 McOwen C.J., Pickering M.D., Reef R., Vafeidis A.T., Hinkel J., Nicholls R.J.,
1018 Brown S., 2018. Future response of global coastal wetlands to sea-level rise.
1019 *Nature* 561, 231-234.

1020 Syvitski J.P.M., Kettner A., Overeem I., Hutton E.W.H., Hannon M.T.,
1021 Brakenridge C.R., Day J., Vorosmarty C., Saito Y., Giosan L., Nicholls R.J.,
1022 2009. Sinking deltas due to human activities. *Nature Geoscience* 2, 681-686.

1023 Takekawa J.Y., Thorne K.M., Buffington K.J., Spragens K.A., Swanson K.M.,
1024 Drexler J.Z., Schoellhamer D.H., Overton C.T., Casazza M.L., 2013. Final
1025 report for sea-level rise response modeling for San Francisco Bay estuary
1026 tidal marshes. U.S. Geological Survey Open File Report 2013-1081,
1027 doi.org/10.3133/ofr20131081.

1028 Talke S.A., Jay D.A., 2020. Changing tides: the role of natural and
1029 anthropogenic factors. *Annual Review of Marine Sciences* 12: 14.1-14.31.

1030 Temmerman S., Meire P., Bouma T.J., Herman P.M.J., Ysebaert T., de Vriend
1031 H.J., 2013. Ecosystem-based coastal defense in the face of global change.

1032 Nature 504, 79-83.

1033 Thorne K., MacDonald G., Guntenspergen G., Ambrose R., Buffington K.,
1034 Dugger B., Freeman C., Janousek C., Brown L., Rosencranz J., Holmquist J.,
1035 2018. US Pacific coastal wetland resilience and vulnerability to sea-level rise.
1036 Science Advances 4(2), p.eaao3270.

1037 Townend I.H., Pethick, J., 2002. Estuarine flooding and managed retreat.
1038 Philosophical Transactions of the Royal Society London A 360(1796),
1039 1477-1495.

1040 Townend I.H., Whitehead P., 2003. A preliminary net sediment budget for the
1041 Humber Estuary. Science of The Total Environment 314-316: 755-767.

1042 Townend I.H., Wang Z.B., Rees J.G., 2007. Millennial to annual volume
1043 changes in the Humber Estuary. Proceedings of the Royal Society A 463,
1044 837-854.

1045 Townend I.H., Wang Z.B., Stive M., Zhou Z., 2016. Development and extension
1046 of an aggregated scale model: part I- background to ASMITA. China Ocean
1047 Engineering 30(4), 483-504.

1048 Valiela I., Lioret J., Bowyer T., Miner S., Remsen D., Elmstrom E., Cogswell C.,
1049 Thieler E.R., 2018. Transient coastal landscapes: rising sea level threatens
1050 salt marshes. Science of The Total Environment 640-641, 1148-1156.

1051 van de Lageweg W.I., Slangen A.B.A., 2017. Predicting dynamic coastal delta
1052 change in response to sea-level rise. Journal of Marine Science and
1053 Engineering 24, 1-12.

1054 van Maanen B., Coco G., Bryan K.R., Friedrichs C.T., 2013. Modeling the
1055 morphodynamic response of tidal embayments to sea-level rise. Ocean
1056 Dynamics, doi: 10.1007/s10236-013-0649-6.

1057 van der Wegen M., Roelvink J.A., 2008. Long-term morphodynamic evolution
1058 of a tidal embayment using a two-dimensional, process-based model.
1059 Journal of Geophysical Research, 113,C03016, doi:10.1029/2006JC003983.

1060 van der Wegen M., 2013. Numerical modeling of the impact of sea level rise on
1061 tidal basin morphodynamics. Journal of Geophysical Research: Earth

1062 Surface 118, 447-460.

1063 van der Wegen M., Jaffe B., Foxgrover A., Roelvink D., 2016. Mudflat
1064 morphodynamics and the impact of sea level rise in South San Francisco
1065 Bay. *Estuaries and Coasts*, doi:10.1007/s12237-016-0129-6.

1066 van Goor M.A., Zitman T.J., Wang Z.B., Stive M.J.F., 2003. Impact of sea-level
1067 rise on the morphological equilibrium state of tidal inlets. *Marine Geology* 202,
1068 211–227.

1069 van Wijnen H.J., Bakker J.P., 2001. Long-term surface elevation change in salt
1070 marshes: a prediction of marsh response to future sea-level rise. *Estuarine,
1071 Coastal and Shelf Science* 52, 381-390.

1072 Wang Z.B., Townend I.H., 2012. Influence of the nodal tide on the
1073 morphological response of estuaries. *Marine Geology* 291-294, 73-82.

1074 Wang Z.B., Elias E.P.L., van der Spek A.J.F., Lodder Q.J., 2018. Sediment
1075 budget and morphological development of the Dutch Wadden Sea: impact of
1076 accelerated sea-level rise and subsidence until 2100. *Netherlands Journal of
1077 Geosciences* 97, 183-214.

1078 Wolanski E., Chappell J., 1996. The response of tropical Australian estuaries
1079 to a sea level rise. *Journal of Marine Systems* 7, 267–279.

1080 Zhao J., Guo L.C. He Q., Wang Z.B., van Maren D.S., Wang X.Y., 2018. An
1081 analysis on half century morphological changes in the Changjiang Estuary:
1082 spatial variability under natural processes and human intervention. *Journal of
1083 Marine Systems* 181, 25-36.

1084 Zhao K., Gong Z., Xu F., Zhou Z., 2019. The role of collapsed bank soil on tidal
1085 channel evolution: a process-based model involving bank collapse and
1086 sediment dynamics. *Water Resources Research* 55,
1087 doi:10.1029/2019WR025514.

1088 Zhang X.H., Leonardi N., Donatelli C., Fagherazzi S., 2020. Divergence of
1089 sediment fluxes triggered by sea-level rise will reshape coastal bays.
1090 *Geophysical Research Letters*, doi: 10.1029/2020GL087862.

1091 Zhou Z., Coco G., Townend I., Olabarrieta M., van der Wegen M., Gong Z.,

1092 D'Alpaos A., Gao S., Jaffe B.E., Gelfenbaum G., He Q., Wang Y.P., Lanzoni
1093 S., Wang Z.B., Winterwerp H., Zhang C.K., 2017. Is 'morphodynamic
1094 equilibrium' and oxymoron? Earth-Science Reviews 165, 257-267.

1095 Zhou Z., Chen L.Y., Tao J.F., Gong Z., Guo L.C., van der Wegen M., Townend
1096 I., Zhang C.K., 2020. The role of salinity in fluvio - deltaic morphodynamics:
1097 A long - term modelling study, Earth Surface Processes and Landforms
1098 45(3), 590-604.

1099